J. Mod. Transport. (2015) 23(3):169–175
DOI 10.1007/s40534-015-0075-1

www.springer.com/40534

Assessment of the curving performance of heavy haul trains under braking conditions

Liangliang Yang[1] · Yu Kang[1] · Shihui Luo[1] · Maohai Fu[2]

Received: 1 November 2014 / Revised: 5 May 2015 / Accepted: 7 May 2015 / Published online: 27 May 2015

Abstract To study the curving performance of trains, 1D and 3D dynamic models of trains were built using numerical methods. The 1D model was composed of 210 simple wagons, each allowed only longitudinal motion; whereas the 3D model included three complicated wagons for which longitudinal, lateral, and vertical degrees of freedom were considered. Combined with the calculated results from the 1D model under braking conditions, the behavior of draft gears and brake shoes were added to the 3D model. The assessment of the curving performance of trains was focused on making comparisons between idling and braking conditions. The results indicated the following: when a train brakes on a curved track, the wheel-rail lateral force and derailment factor are greater than under idling conditions. Because the yawing movement of the wheelset is limited by brake shoes, the zone of wheel contact along the wheel tread is wider than under idling conditions. Furthermore, as the curvature becomes tighter, the traction ratio shows a nonlinear increasing trend, whether under idling or braking conditions. By increasing the brake shoe pressure, train steering becomes more difficult.

Keywords Heavy haul train · Curving performance · Draft gear · Brake shoe · Wheel-rail · Derailment safety · Wheel wear power · Traction ratio

✉ Liangliang Yang
yll137@126.com

[1] Traction Power State Key Laboratory, Southwest Jiaotong University, Chengdu 610031, China

[2] School of Mechanical Engineering, Southwest Jiaotong University, Chengdu 610031, China

1 Introduction

With the rapid development of heavy haul railways, an increase in wagon number of heavy haul trains has been an important way to improve transportation capacity. However, the longer a train is, the more time it generally takes to decelerate or stop. Thus, greater longitudinal impulses may occur between adjacent wagons. Based on extensive theoretical and experimental research, problems such as damage to the vehicle structure and train derailments were found to be caused by the longitudinal impulses from train braking. To solve these problems, many scholars included train braking conditions when assessing train performance, especially the curving performance of trains. Durali and Ahadmehri [1] studied the derailment coefficient of a five-car train under emergency braking conditions, modeling with complete degrees of freedom (DOFs), but the calculations involved excessive computational costs. Zhang et al. [2–4] discussed safety and comfort indexes under idling, traction, and braking conditions for a long and heavy haul train. His circular variable method was acknowledged as a low-cost approach to simulating train system dynamics. Pugi et al. [5] focused on the relationship between coupler force and relative load reduction. His work was performed using multi-body dynamics and pneumatics methods. Ma et al. [6], Wu et al. [7], and Xu et al. [8]. showed that the wheelset lateral force would vary with coupler compression and rotation when the electric brake was operated on a tangent or curved track. Cole et al. [9]. demonstrated that wheel load reduction occurred during train braking, in which nodding movement between the rail car body and bogie was taken into account. Sun et al. [10] and Liu and Wei [11] reported that derailment indexes change with the coupler deflection angle when a train of 10,000 tons proceeded around a curve with air brake operation.

In these previous research efforts, attention was paid to the relationship between draft gear behavior and wheel-rail interaction, but the effect from the brake shoe pushing the wheel tread was usually of less concern. In this study, dynamic models of 1D and 3D trains were established using numerical methods, in which the dynamic behaviors of draft gears and brake shoes were both considered. The assessment of the curving performance of trains focused more on making comparisons between idling and braking conditions. Furthermore, this study provides a feasible approach to solving the rapidly increasing freedoms considered in train system dynamics.

2 1D train model

The train under consideration was equipped with 2 HX_{D2} locomotives and 210 C_{80} wagons. Used on the Datong–Qinhuangdao line, the electric locomotive and the coal gondola were both heavy haul freight cars with 25 t axle loading. In the 1D train model, all cars were simplified as a series of mass points that allowed only longitudinal motion. Also each car was subject to a coupler force from the draft gear, a basic propulsion force and an air brake force. These forces, whether from the locomotive or wagon, can be described by different equations. Moreover, only traction and dynamic brake forces were added to each locomotive.

The traction or dynamic brake system is complex, because many factors need to be considered, such as limited output power, limited torque from the thermal effect, and limited wheel-rail adhesion. Based on the above limiting factors, traction and dynamic brake characteristics can be achieved by fitting a piecewise linear function to the curve, as shown in Fig. 1.

Air brake forces mainly depend on the value of pressure rising in the brake cylinder, and the rising characteristic also depends on how much the pressure reduction is in the brake pipe. As shown in Fig. 2, pressure increases in the brake cylinder can be obtained from different pressure reductions in the air brake test. Moreover, rising pressure is subject to delay and attenuation because of the air wave traveling from one car to another. Accordingly the air brake force of each car can be given by

$$F_{\mathrm{B}} = n \times S \times \lambda \times \eta \times \varphi \times f(t), \tag{1}$$

where F_{B} is the air brake force of each car, n the number of brake cylinders, S the area of the cylinder piston, λ the brake leverage, η the transmission efficiency, φ the equivalent friction coefficient of a brake shoe, and $f(t)$ the function of pressure rising in the brake cylinder.

The basic propulsion force is usually defined as the sum of the running, curving, and gradient resistances. The running resistance is expressed by an empirical formula, which is composed of friction resistance and air resistance. Curving resistance is also included by another empirical formula related only to the curve radius. The gradient resistance is the parallel component of the vehicle weight. Thus the basic propulsion force can be defined as

$$F_{\mathrm{W}} = G\left[\left(A + BV + CV^2\right) + (600/R) + i\right], \tag{2}$$

where F_{W} is the total basic propulsion force in Newtons, G is the gross vehicle weight in kiloNewtons, A, B, and C are the relevant coefficients for the running resistance, V is the velocity of the car in kilometers per hour, R is the curve radius in meters, and i is the thousandth of the gradient.

The hysteresis characteristic of the draft gear unit can be expressed by a force–displacement curve. As shown in Fig. 3, it is described by a coupler slack, preload, loading line, unloading line, and transition line. To obtain a steady switching response from loading to unloading, a modified index control method [12] was adopted.

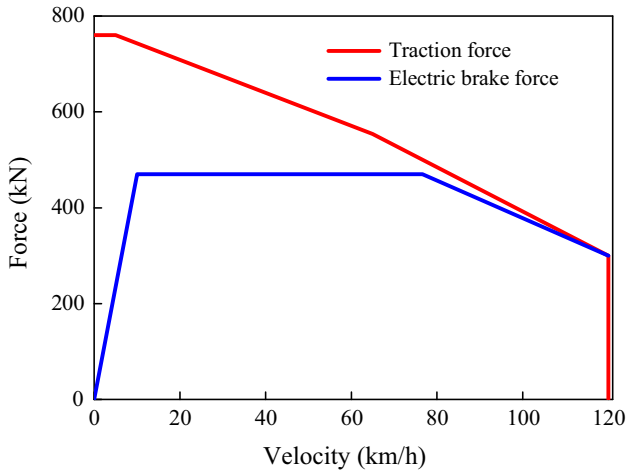

Fig. 1 Characteristics of traction and dynamic brake forces

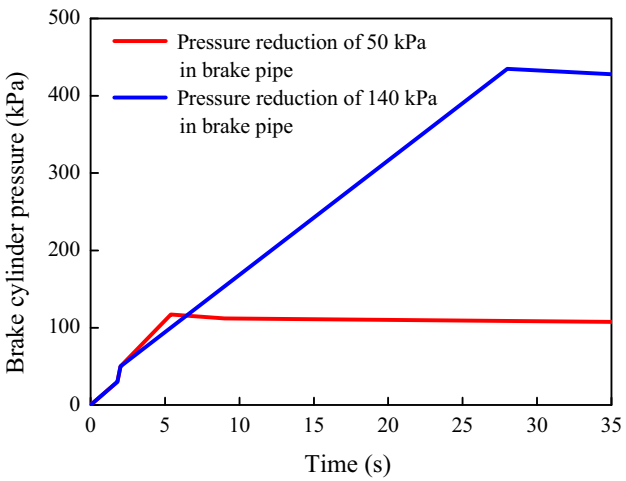

Fig. 2 Rising characteristics of brake cylinder pressure

According to the simplification above, the 1D train dynamic model was established using MATLAB/SIMULINK software [13]. It was only able to solve longitudinal dynamic problems. However, no matter which car of the train is under consideration, the coupler force and brake shoe pressure that varied with braking time can easily be obtained.

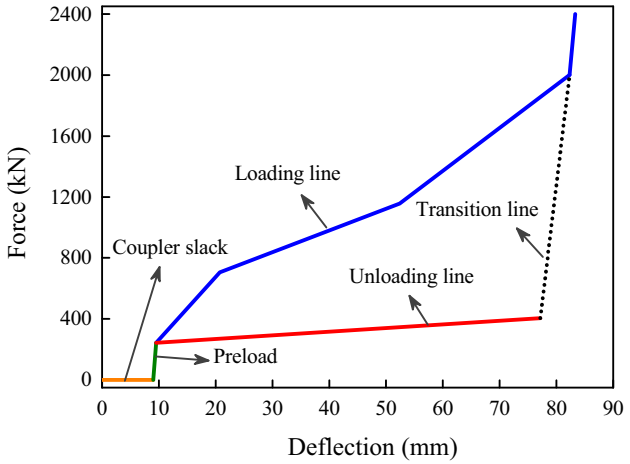

Fig. 3 Characteristic curve of draft gear

3 3D train model

The 3D train model included three complicated wagons for which the longitudinal, lateral, and vertical DOFs were considered. Each wagon was composed of a C_{80} type stainless steel car body and a ZK6 type three-piece bogie. Specifically, the detailed vehicle system was mainly made up of several rigid bodies including the car body, bolster, side frame, adapter, wheelset, and coupler. It also contained some stiffness and damping components such as the rubber pad, coil spring, frictional wedge, side bearing, cross supporting bar, and buffer. In addition, the FASTSIM algorithm was applied to calculating the creep force of the wheel-rail. Furthermore, the dynamic behavior of the coupler and additional constraints from the brake shoe pressure were also taken into account. As shown in Fig. 4,

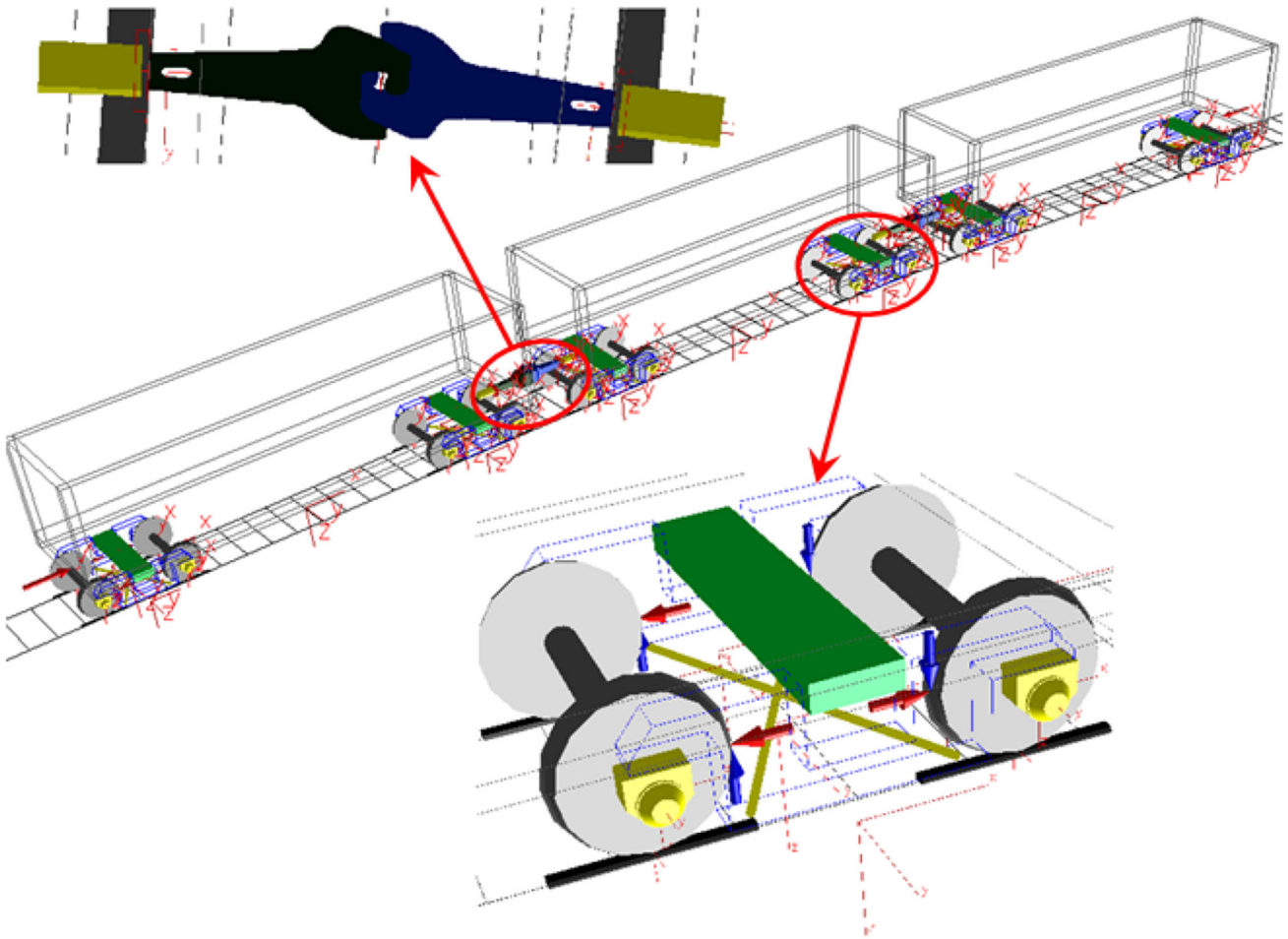

Fig. 4 Train dynamics model with complete DOFs

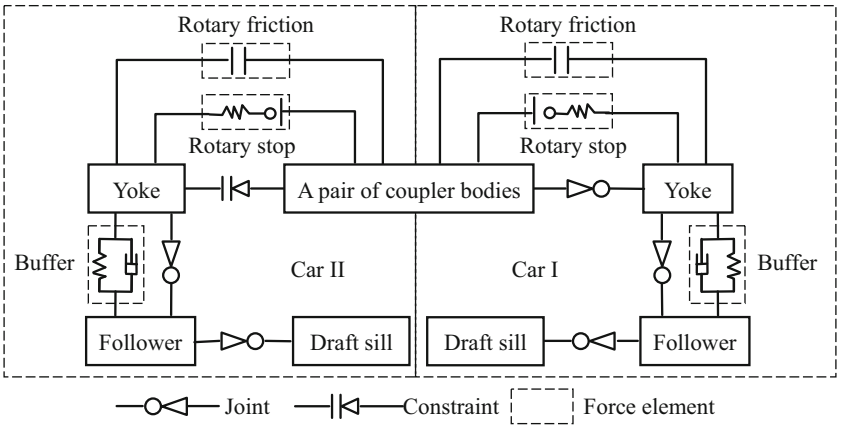

Fig. 5 Topological relationships in the coupler and buffer system

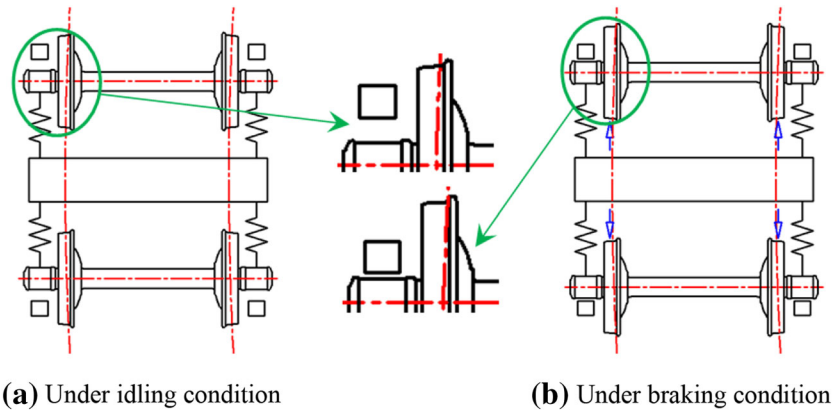

(a) Under idling condition **(b)** Under braking condition

Fig. 6 Diagram of bogie passing through tight curve

the 3D train dynamic model was built using the SIMPACK software.

The mechanical movement of the 17 type coupler and MT-2 type buffer device was too complex, so their connection was simplified into topologic relationships between several major components, such as the coupler body, yoke, follower, and buffer. A brief illustration of the topologic relationships in the coupler and buffer system is shown in Fig. 5.

When the train passes around a curve, a horizontal rotary angle will occur between the coupler body and car body in the direction of the longitudinal centerline, but it is limited by the structural dimensions of the coupler. Once the angle reaches the maximum, a rigid contact will occur between the coupler shoulder and coupler carrier, avoiding excessive lateral deflection. Thus the restoring torque from a rotary stop is given by

$$\begin{cases} T_{\mathrm{b}} = 0, & |\alpha| \le \theta_{\max}, \\ T_{\mathrm{b}} = k_{\mathrm{b}}[\alpha - \mathrm{sign}(\alpha)\theta_{\max}], & |\alpha| > \theta_{\max}, \end{cases} \tag{3}$$

where T_{b} is the restoring torque, k_{b} the restoring stiffness, α the rotary angle, $\theta_{\max}$ the maximum value of the rotary angle, and $\mathrm{sign}(\alpha)$ the sign function of α.

If the draft gear is subjected to compression and rotation, the rotary friction of the coupler will work between the convex surface in the coupler tail and the concave surface in the follower. The friction force or torque plays an important role in limiting lateral deflection, especially when the car bears a large compressing force. Based on the theory of stick–slip friction, the rotary friction force can be expressed as

$$\begin{cases} f = 0, & F_{\mathrm{c}} \le 0, \\ f = cs_{ij} + dv_{ij}, & 0 \le |v_{ij}| \le v_{\mathrm{switch}} \text{ and } |f| \le u_{\mathrm{stick}} F_{\mathrm{c}}, \\ f = \mathrm{sign}(v_{ij}) u_{\mathrm{slip}} F_{\mathrm{c}}, & |v_{ij}| > v_{\mathrm{switch}} \text{ or } |f| > u_{\mathrm{stick}} F_{\mathrm{c}}, \end{cases} \tag{4}$$

where F_{c} is the normal force of the coupler tail, f is the friction force of the coupler tail, c and d are the equivalent stiffness and damping of the stick friction, s_{ij} and v_{ij} are the relative displacement and velocity, v_{switch} is the shift velocity between the stick and slip friction, μ_{stick} is the coefficient of the stick friction, μ_{slip} is the coefficient of the slip friction, and $\mathrm{sign}(v_{ij})$ is the sign function of v_{ij}.

In addition, the braking on wheel tread is generally applied to the three-piece bogie. This type of foundation

brake rigging is a linkage assembly including the middle pull rod and the unilateral brake shoe. When the train brakes, each brake shoe is pushed to the wheel tread from inside to outside. It not only slows down rotational movement of the wheelset, but also limits its stretching and yawing movements. In Fig. 6, when a bogie brakes on a tight curve, the longitudinal gap between the guide wheel and side frame reduces greatly because of the brake shoe pressure, so it is more difficult for the wheelset to move to the radial position.

To simplify the complex transmission mechanism, mechanical relationships of the free lever, dead lever, and brake shoe can be simulated by inputting concentrated forces over braking time. In particular, the forces from the brake shoe and the free or dead lever must meet the actual braking leverage. In addition, the brake shoe force can be decomposed into the contact force and the friction force.

4 Calculation and analysis

As coupler force and brake shoe pressure from the 1D train model are added, the 3D train model with detailed modeling can solve lateral and vertical problem of a heavy haul train. In this study, the simulation results focus on the derailment safety, wheel wear power, and traction ratio.

4.1 Derailment safety

The train runs on a circle curve of R300, and maintains its initial speed of 60 km/h. Without losing generality, the 30th car of the train is selected as the simulated car. As shown in Fig. 7, when service braking is operated, coupler forces from neighboring cars show similar trends. However, the variation in the coupler force with a pressure reduction of 50 kPa is different from that with a pressure

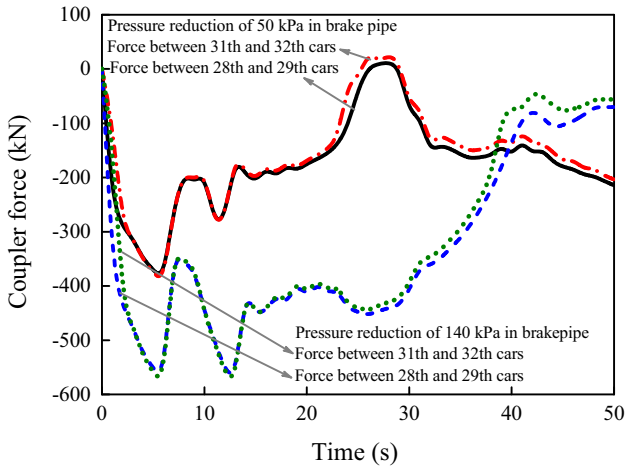

Fig. 7 Force-time history of couplers

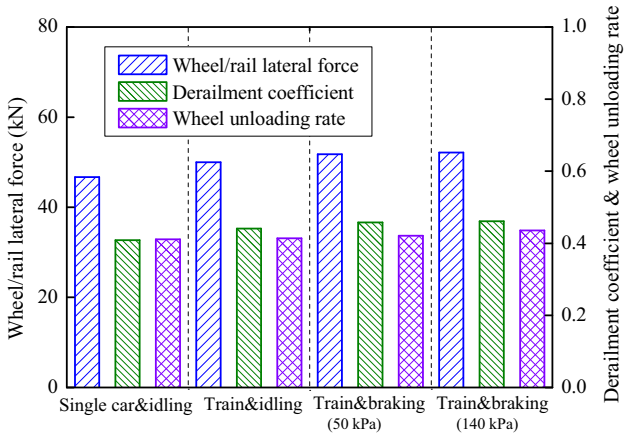

Fig. 8 Safety indexes under different running conditions

reduction of 140 kPa. Significantly, the longitudinal impulse caused by the latter is much greater.

To study the effects of the coupler and brake shoe, a single car model and train model were established. These models were simulated on track with the 5th grade irregularity of U.S. railways. The results for the wheel-rail lateral force, derailment coefficient, and wheel unloading rate are shown in Fig. 8. Because of the additional lateral force from coupler compression and rotation, the wheel-rail lateral force and derailment coefficient in the train model were 7.1 % and 7.8 % greater than those in the single car model. Because of the additional yawing constraint from brake shoe pressure, the wheel-rail lateral force and derailment coefficient in the train braking model were both greater than in the train idling model. In particular, when the pressure reduction in the train pipe was set to 140 kPa, there were about 4.3 % and 4.5 % increases in the wheel-rail lateral force and derailment coefficient. Because the effect caused by the coupler or brake shoe in the vertical direction was very small, the wheel unloading rates remained nearly the same under all running conditions. Compared with the coupler force, the effect of brake shoe pressure was relatively weak, but it was still an important factor in degrading derailment safety.

4.2 Wheel wear power

When applied in engineering, wheel wear power is often used to assess the friction work from the wheel-rail contact spot. More serious wear usually occurs on a tight curve, thus the study into the wear power of the guide wheel was simulated on the S type curve of R300, as shown in Fig. 9.

Figure 9 shows the distribution of wheel wear power under different running conditions. The wear power in the train model was greater than in the single car model, while the distribution characteristics were nearly the same in both models. It was noticed that the range of wheel contact

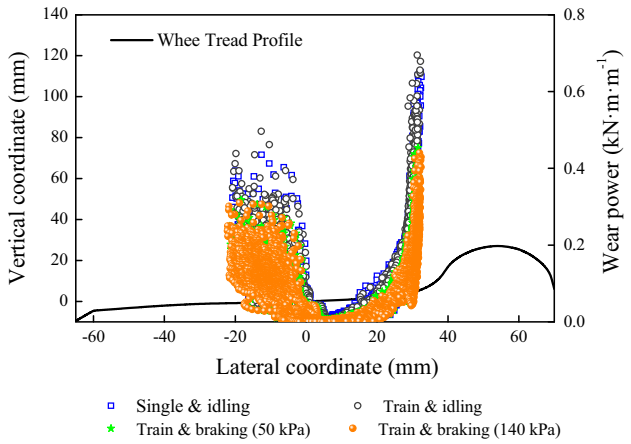

Fig. 9 Distributions of wear power under different running conditions

along the wheel tread in the train braking model was wider than in the train idling model. Because the yawing movement of the guide wheelset was limited by the brake shoe, it was inevitable that the angle of attack reduced. Meanwhile, as the train slowed down, the average wear power decreased. However, it was inevitable that more serious wear occurred on the root of the flange when train braking was operated on a curved track.

4.3 Traction ratio

During curve negotiation, the creep force from the wheel-rail cannot be regarded as only the driving force for guidance [14, 15] but is also the rolling resistance for traction. Therefore an appropriate creep condition is helpful in keeping safer steering capability and lower energy consumption. Since 2010, the Transportation Technology Center, Inc. has been tasked by the Association of American Railroads to develop and evaluate a better three-piece bogie for a heavy haul freight car. One of the important objectives was to reduce the wheel-rail rolling resistance in steering operation. Based on a considerable amount of theoretical and experimental research [16, 17], the traction ratio *T*/*N* was defined as the quantitative index for rolling resistance, which was associated with the interaction forces between the guide wheelset and low rail. The specific definition can be expressed as

$$\begin{cases} T_x = -f_{11}\left(\dfrac{\lambda y_w}{r_0} + \dfrac{b\dot{\varphi}_w}{v}\right), \\ T_y = -f_{22}\left(\dfrac{\dot{y}_w}{v} - \varphi_w\right) - f_{23}\left(\dfrac{\lambda}{r_0} + \dfrac{\dot{\varphi}_w}{v}\right), \\ T/N = \dfrac{\sqrt{(T_x)^2 + (T_y)^2}}{N}, \end{cases} \tag{5}$$

where T_x is the longitudinal creep force, T_y is the lateral creep force, T is the total creep force, N is the contact force from the wheel-rail, f_{11} is the longitudinal creep coefficient, f_{22} is the lateral creep coefficient, f_{23} is the spin creep coefficient, λ is the equivalent conicity of the wheel tread, T/N is the traction ratio, y_w and φ_w are the transverse and yawing displacements, $\dot{y}_w$ and $\dot{\varphi}_w$ are the transverse and yawing velocities of the wheelset, r_0 is the wheel radius, and v is the forward speed of the wheelset.

As shown in Fig. 10, the traction ratio on the curved track was clearly greater than on the tangent track, because the former value was composed of the latter and additional values caused by the curvature. The traction ratio on the transition curve was slightly greater than on the circle curve, and was caused by the centrifugal acceleration during the train's movement from the transition curve to the circle curve. When the train entered the circle curve, the traction ratio gradually stabilized at a constant value.

Generally, the influence of the tangent resistance should be removed from the curve resistance results to determine the resultant resistance resulting only from the curving [18]. Consequently, the following analysis was simulated on a circle curve, and the final stable value was selected as the traction ratio for the curving resistance.

Figure 11 indicates that the traction ratio varied with different curvature, in which the higher degree meant a tighter curve [19]. As the curvature tightened, the traction ratio showed a nonlinear increasing trend, whether under idling or braking conditions. When the train braking was operated, the front and back wheelsets were limited by the brake shoes. As a result, the longitudinal displacements from the free and elastic deformation no longer contributed to the steering. In addition, the traction ratio showed a slight increase with the increase in the brake shoe pressure. Although the effect from the brake shoe pressure on the

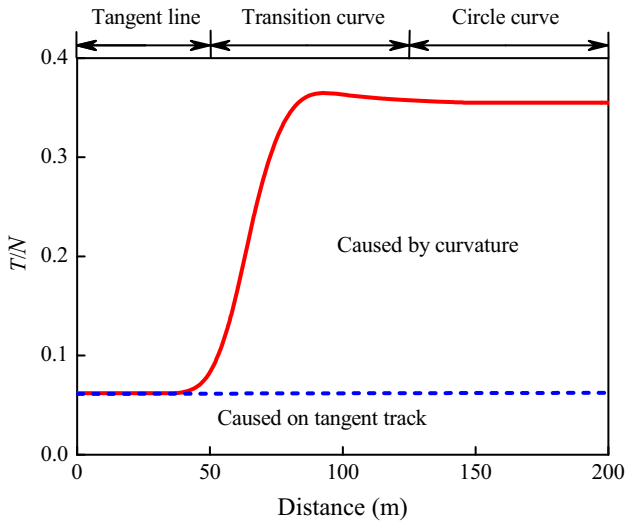

Fig. 10 Traction ratios during dynamic curving

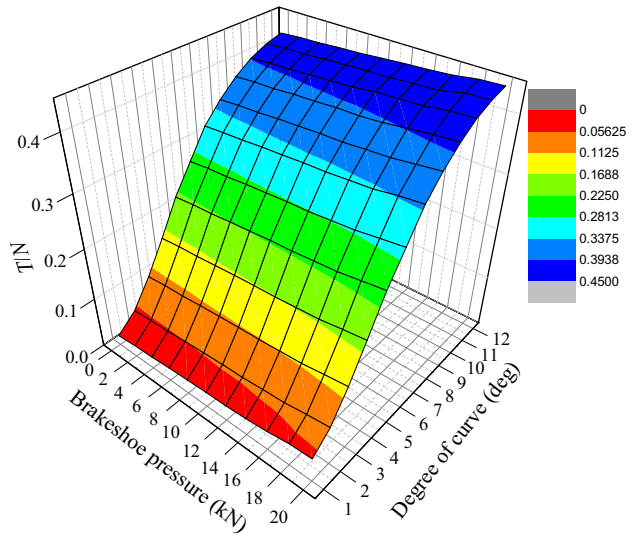

Fig. 11 Traction ratios with different brake shoe pressures

rolling resistance for each car was very small, it was significant in assessing the whole energy consumption of the heavy haul train.

5 Conclusions

(1) Because of the additional lateral force from the coupler compression and rotation, the wheel-rail lateral force and derailment coefficient in the train model were 7.1 % and 7.8 % greater than those in the single car model. Because of the additional yawing constraint from the brake shoe pressure, the wheel-rail lateral force and derailment coefficient in the train braking model with a pressure reduction of 140 kPa were 4.3 % and 4.5 % greater than those in the train idling model.

(2) The wear power in the train model was greater than in the single car model, but the distribution characteristics in the two models were nearly the same. Unfortunately, the range of wheel contact along the wheel tread in the train braking model was wider than in the train idling model.

(3) As the curvature tightened, the traction ratio showed a nonlinear increasing trend, whether under idling or braking conditions. In addition, the traction ratio showed a slight increase with an increase in the brake shoe pressure.

References

1. Durali M, Shadmehri B (2003) Nonlinear analysis of train derailment in severe braking. J Dyn Syst Meas Contr 125(1):48–53
2. Zhang W H, Chi M R, Zeng J 2005 A new simulation method for the train dynamics. 8th International Heavy Haul Conference,Rio de Janeiro, pp 773–778
3. Chi MR, Zhang WH, Zeng J et al (2007) Mixed marshalling influence of light vehicles and heavy vehicles on train stability. J Traffic Transp Eng 7(2):10–13 **(in Chinese)**
4. Chi MR, Jiang YP, Zhang WH et al (2011) System dynamics of long and heavy haul train. J Traffic Transp Eng 11(3):34–40 **(in Chinese)**
5. Pugi L, Rindi A, Ercole AG et al (2011) Preliminary studies concerning the application of different braking arrangements on Italian freight trains. Veh Syst Dyn 49(8):1339–1365
6. Ma WH, Luo SH, Song RR (2012) Coupler dynamic performance analysis of heavy haul locomotives. Veh Syst Dyn 50(9):1435–1452
7. Wu Q, Luo SH, Xu ZQ et al (2013) Coupler jackknifing and derailments of locomotives on tangent track. Veh Syst Dyn 51(11):1784–1800
8. Xu ZQ, Ma WH, Wu Q et al (2013) Coupler rotation behaviour and its effect on heavy haul trains. Veh Syst Dyn 51(12):1818–1838
9. Cole C, Spiryagin M, Sun YQ (2013) Assessing wagon stability in complex train systems. Int J Rail Transp 1(4):193–217
10. Sun SL, Li F, Huang YH et al (2013) Numerical simulation of impact effect on heavy haul train. J Vib Shock 32(10):69–73 **(in Chinese)**
11. Liu S, Wei W (2014) Research on the unsteady influence model of the heavy haul train for safe running. J Mech Eng 50(10):127–142 **(in Chinese)**
12. Chang CY, Wang CG, Ma DW et al (2006) Study on numerical analysis of longitudinal forces of the T20,000 heavy haul. J China Railw Soc 28(2):89–94 **(in Chinese)**
13. Yang LL, Luo SH, Fu MH et al (2014) Study on effect of longitudinal impulse for 20,000 t heavy combined train. Electr Drive Locomot 3:34–39 **(in Chinese)**
14. Wang FT (1994) Vehicle system dynamics. China Railway Publishing House, Beijing
15. Yan JM, Fu MH (2008) Vehicle engineering. China Railway Publishing House, Beijing
16. Tournay H (2013) Development and evaluation of next generation integrated freight truck designs in North America. 10th International Heavy Haul Conference, New Delhi, pp 713–721
17. Transportation Technology Center, Inc. (2013) 18th Annual AAR Research Review. Pueblo: The Association of American Railroads
18. The Association of American Railroads (2007) AAR M-976-2006 truck performance for rail cars. AAR Safety and Operations, Washington, DC
19. The Association of American Railroads (2007) AAR M-1001-2007 design, fabrication, and construction of freight cars. AAR Safety and Operations, Washington, DC